

# Journal of Visualized Experiments

## A Microfluidic System with Surface Patterning for Investigating Cavitation Bubble(s)-Cell Interaction and Resultant Bioeffects at Single Cell Level

--Manuscript Draft--

<b>Manuscript Number:</b>	JoVE55106R1
<b>Full Title:</b>	A Microfluidic System with Surface Patterning for Investigating Cavitation Bubble(s)-Cell Interaction and Resultant Bioeffects at Single Cell Level
<b>Article Type:</b>	Invited Methods Article - JoVE Produced Video
<b>Keywords:</b>	Microfluidics; single cell analysis; cavitation; cell patterning; jetting flow; membrane poration; membrane deformation; calcium response.
<b>Manuscript Classifications:</b>	5.5.830: Rheology; 5.5.830.666: Microfluidics; 7.1.154: Biophysical Phenomena; 7.1.154.100: Biophysical Processes; 7.1.154.100.440: Mechanotransduction, Cellular; 93.34.7: cavitation
<b>Corresponding Author:</b>	Fenfang Li Duke University Durham, NORTH CAROLINA UNITED STATES
<b>Corresponding Author Secondary Information:</b>	
<b>Corresponding Author E-Mail:</b>	fenfang.li@duke.edu
<b>Corresponding Author's Institution:</b>	Duke University
<b>Corresponding Author's Secondary Institution:</b>	
<b>First Author:</b>	Fenfang Li
<b>First Author Secondary Information:</b>	
<b>Other Authors:</b>	Fang Yuan Georgy Sankin Chen Yang Pei Zhong
<b>Order of Authors Secondary Information:</b>	
<b>Abstract:</b>	In this manuscript, we first describe the fabrication protocol of a microfluidic chip with gold dots and fibronectin-coated regions on the same glass substrate to precisely control the generation of tandem bubbles and individual cells patterned nearby with well-defined location and shape. We then demonstrate the generation of tandem bubbles by using two pulsed lasers illuminating on a pair of gold dots with a few microsecond time delay. We visualize the bubble-bubble interaction and jet formation by high-speed imaging and characterize the resultant flow field using particle image velocimetry (PIV). Finally, we present some applications of using this technique for single cell analysis, including cell membrane poration with macromolecule uptake, localized membrane deformation determined by the displacements of attached integrin-binding beads, and intracellular calcium response from ratiometric imaging. Our results show that a fast and directional jetting flow is produced by the tandem bubble interaction, which can impose a highly localized shear stress on the surface of a cell grown in close proximity. Furthermore, different bioeffects could be induced by altering the strength of the jetting flow by adjusting the standoff distance from the cell to the tandem bubbles.
<b>Author Comments:</b>	
<b>Additional Information:</b>	
<b>Question</b>	<b>Response</b>

If this article needs to be "in-press" by a certain date to satisfy grant requirements, please indicate the date below and explain in your cover letter.

**TITLE:**

A Microfluidic System with Surface Patterning for Investigating Cavitation Bubble(s)-Cell Interaction and the Resultant Bioeffects at the Single-Cell Level

**AUTHORS:****Li, Fenfang**

Mechanical Engineering and Materials Science  
Duke University  
Durham, NC, USA  
Fenfang.li@duke.edu

**Yuan, Fang**

CytoTheraX Inc.  
Natick, MA, USA  
fang@cytotherax.com

**Sankin, Georgy**

Mechanical Engineering and Materials Science  
Duke University  
Durham, NC, USA  
georgy.sankin@duke.edu

**Yang, Chen**

Mechanical Engineering and Materials Science  
Duke University  
Durham, NC, USA  
chen.yang2@duke.edu

**Zhong, Pei**

Mechanical Engineering and Materials Science  
Duke University  
Durham, NC, USA  
pzhong@duke.edu

**CORRESPONDING AUTHOR:**

Li, Fenfang  
Fenfang.li@duke.edu

**KEYWORDS:**

Microfluidics; single-cell analysis; cavitation; cell patterning; jetting flow; membrane poration; membrane deformation; calcium response.

**SHORT ABSTRACT:**

A microfluidic chip was fabricated to produce pairs of gold dots for tandem bubble generation

and fibronectin-coated islands for single-cell patterning nearby. The resultant flow field was characterized by particle image velocimetry and was employed to study various bioeffects, including cell membrane poration, membrane deformation, and intracellular calcium response.

#### **LONG ABSTRACT:**

In this manuscript, we first describe the fabrication protocol of a microfluidic chip, with gold dots and fibronectin-coated regions on the same glass substrate, that precisely controls the generation of tandem bubbles and individual cells patterned nearby with well-defined locations and shapes. We then demonstrate the generation of tandem bubbles by using two pulsed lasers illuminating a pair of gold dots with a few-microsecond time delay. We visualize the bubble-bubble interaction and jet formation by high-speed imaging and characterize the resultant flow field using particle image velocimetry (PIV). Finally, we present some applications of this technique for single cell analysis, including cell membrane poration with macromolecule uptake, localized membrane deformation determined by the displacements of attached integrin-binding beads, and intracellular calcium response from ratiometric imaging. Our results show that a fast and directional jetting flow is produced by the tandem bubble interaction, which can impose a highly-localized shear stress on the surface of a cell grown in close proximity. Furthermore, different bioeffects can be induced by altering the strength of the jetting flow by adjusting the standoff distance from the cell to the tandem bubbles.

#### **INTRODUCTION:**

There is a growing recognition that cellular heterogeneity, arising from the stochastic expression of genes, proteins, and metabolites, exists within a large cell population and serves as a fundamental principle in biology to allow for cell adaptation and evolution<sup>1</sup>. Therefore, it is often inaccurate and unreliable to use population-based bulk measurements to understand the function of individual cells and their interactions. Developing new technologies for single-cell analysis is therefore of high interest in biological and pharmacological research, and can be used, for example, to better understand the key signaling pathways and processes in stem cell biology and cancer therapy<sup>2-4</sup>. In recent years, the emergence of microfluidic platforms has greatly facilitated single-cell analysis, where the positioning, treatment, and observation of the response from individual cells have been performed with novel analytical strategies<sup>5</sup>.

Cavitation plays an important role in a diverse range of biomedical applications, including the treatment of cancers by high-intensity focused ultrasound (HIFU)<sup>6</sup>, the non-invasive fragmentation of kidney stones by shock wave lithotripsy (SWL)<sup>7</sup>, drug or gene delivery by sonoporation<sup>8</sup>, and the recently-reported destruction of cells or tissues by hydrodynamic bubble cavitation<sup>9,10</sup>. Despite this, the dynamic processes of cavitation bubble(s) interactions with biological tissue and cells have not been well understood. This is due to the randomness in cavitation initiation and bubble dynamics produced by ultrasound, shock waves, and local hydraulic pressure; furthermore, there is a lack of enabling techniques to resolve the inherently complex and fast responses of biological cells, especially at the single-cell level.

Because of these challenges, it is not surprising that very few studies have been reported to investigate bubble-cell interactions under well-controlled experimental conditions. For

example, membrane poration of individual cells trapped in suspension<sup>11</sup> and the impulsive large deformation of human red blood cells<sup>12</sup> have been demonstrated using laser-generated single bubbles in microfluidic channels. The latter technique, however, can only produce very small deformation in eukaryotic cells because of the presence of the nucleus<sup>13</sup>. Moreover, it is difficult to monitor downstream bioeffects when treating cells in suspension. In other studies, ultrasound excitation of a cell-bound microbubble (or ultrasound contrast agent) for producing membrane poration and/or intracellular calcium responses in single adherent cells has been reported<sup>8</sup>. Membrane poration of single adherent cells can also be produced by using laser-generated tandem bubbles in a thin liquid layer containing light-absorbing Trypan blue solution<sup>14</sup>, or by an oscillating gas bubble generated by microsecond laser pulses irradiating through an optically-absorbing substrate in microchambers<sup>15</sup>. When compared, the optically-absorbing substrate has an advantage over the laser-absorbing Trypan blue solution because the latter is toxic to cells. More importantly, laser-generated bubbles are more controllable in terms of bubble size and location than acoustically-excited bubbles. Nevertheless, in all these previous studies, the cell shape, orientation, and adhesion conditions were not controlled, which may substantially influence the cell response and bioeffects produced by mechanical stresses<sup>16</sup>.

To overcome these drawbacks in previous studies, we have recently developed an experimental system for bubble generation, cell patterning, bubble-bubble-cell interactions, and real-time bioassays of cell response in a microfluidic chip constructed by using a unique combination of microfabrication techniques. Three main features that distinguish our experimental system from others in the field are: 1) the patterning of micron-sized gold dots on the glass substrate to enable localized laser absorption for bubble generation<sup>17</sup>; 2) the patterning of micron-sized islands of extracellular matrix (ECM) for cell adhesion on the same substrate to control both the location and geometry of individual cells; and 3) the compression of the dimension of the bubble-bubble-cell interaction domain from 3D to a quasi-2D space to facilitate in-plane visualization of bubble-bubble interactions, jetting flow fields, cell deformation, and bioeffects, all captured in one streamlined imaging sequence (Figure 1d).

[Place Figure1 here]

This platform can be further combined with fluorescence assays and functionalized beads attached to the cell surface for cavitation-induced bioeffects. In particular, this platform opens the way for reliable and quantifiable assays at the single-cell level. Up to now, we have used the device for the analysis of tandem bubble-induced cell membrane deformation, cell poration and intracellular uptake, viability, apoptosis, and intracellular calcium response. In the following protocol, we describe the process of chip fabrication and the procedure for analyzing the various bioeffects mentioned above. Moreover, the operations of the chip are also described.

## **PROTOCOL:**

### **1. Microfabrication**

Note: All the microfabrication procedures are performed in a cleanroom. A chrome mask is

designed prior to the microfabrication, see Figure 2.

[Place Figure 2 here]

### **1.1) Gold dot patterning**

Note: The area of each gold dot is designed to be within  $25\text{-}30\text{ }\mu\text{m}^2$ , so that it is large enough to absorb laser energy for bubble generation, but small enough to avoid individual cells adhering to it. A schematic diagram for the gold dot fabrication is shown in Figure 3a.

#### **1.1.1) Glass slide cleaning (in a chemical hood)**

1.1.1.1) Flush the glass slide with acetone followed by isopropyl alcohol (IPA), and then dry it with  $\text{N}_2$  flow.

1.1.1.2) Soak the slide in piranha solution ( $\text{H}_2\text{SO}_4\text{:H}_2\text{O}_2 = 4\text{:}1$ ) for 10 min.

1.1.1.3) Take out the slide, rinse it with DI water, and then dry it with  $\text{N}_2$  flow.

1.1.1.4) Bake the glass slide on a hotplate at  $120\text{ }^\circ\text{C}$  for 10 min.

1.1.1.5) Treat the slide in a plasma asher at 100 W for 90 s.

#### **1.1.2) Spin-coating (spin-coating hood)**

1.1.2.1) Turn on a hotplate and wait until the temperature is stable at  $95\text{ }^\circ\text{C}$ .

1.1.2.2) Follow the coating procedure:

1,000 rpm for 5 s with a 500-rpm/s ramp;  
then 3,000 rpm for 30 s with a 1,000-rpm/s ramp.

1.1.2.3) Fix the cleaned glass slide onto the spin coater by applying a vacuum.

1.1.2.4) Cover the slide surface with P-20 and start the coating recipe.

1.1.2.5) Repeat the coating process for NFR-negative photoresist.

1.1.2.6) Bake the slide at  $95\text{ }^\circ\text{C}$  for 60 s and wait until it cools down to room temperature.

#### **1.1.3) Photolithography**

1.1.3.1) Mount the chrome mask onto the mask aligner and make sure that the pattern side is facing down towards the slide.

1.1.3.2) Set the photolithography recipe to hard exposure mode with 9 s of UV exposure and quickly align the glass substrate with the mask.

1.1.3.3) After carrying out the UV exposure, bake the slide at  $95\text{ }^\circ\text{C}$  for 1 min, and then let it

cool down to room temperature.

#### **1.1.4) Development**

1.1.4.1) Develop the pattern on the slide in developer solution while maintaining agitation for 60 s.

1.1.4.2) Remove the slide from the developer, flush it with DI water, and dry it with N<sub>2</sub> flow.

1.1.4.3) Check the pattern geometry under a microscope, and measure and record the feature size.

#### **1.1.5) Gold deposition (E-beam evaporation) and lift-off**

1.1.5.1) Bake the slide at 120 °C for 5 min, and let it cool down to room temperature.

1.1.5.2) Clean the slide with plasma in the reactive ion etching (RIE) machine for 90 s at 500 Torr and 100 W.

1.1.5.3) Deposit 5 nm of Ti and 15 nm of Au onto the slide using an E-beam evaporator<sup>17</sup>.

1.1.5.4) Soak the slide overnight in a glass beaker containing photoresist remover solvent to remove the gold resting on top of the NFR resist.

1.1.5.5) Retrieve the slide, flush it with acetone followed by IPA, and dry it with N<sub>2</sub> flow.

1.1.5.6) Dry the slide on a hot plate at 115 °C before cleaning it in the oxygen plasma asher at 100 W for 90 s.

### **1.2) Molecular-assembly patterning by lift-off (MAPL)**

Note: The area of each fibronectin-coated island is set to be within 700-900 μm<sup>2</sup> to facilitate adequate HeLa cell spreading in a square region while minimizing the chances of multiple cells aggregating on the island. A schematic diagram for the preparation of cell-patterning islands is shown in Figure 3b.

#### **1.2.1) Spin coating**

1.2.1.1) Repeat step 1.1.2, but use S1813-positive photoresist and a temperature of 115 °C.

#### **1.2.2) Aligned photolithography**

1.2.2.1) Mount the chrome mask onto the mask aligner and make sure that the side with the pattern is facing down towards the slide with the gold dots.

1.2.2.2) Set the photolithography recipe to hard exposure mode with 9 s of UV exposure.

1.2.2.3) Align the top mask with the bottom slide using alignment marks, located around the edge of the mask, as a spatial reference.

1.2.2.4) Check the central portion of the mask and verify that the pattern features are aligned correctly.

1.2.2.5) Complete the UV exposure without a post-bake.

### **1.2.3) Development**

1.2.3.1) Repeat step 1.1.3 but with 45 s of development before drying on a hotplate and preserving in N<sub>2</sub> storage.

### **1.3) Chemical treatment**

1.3.1) Prepare the passivating solution: 0.5 mg/mL PLL-g-PEG in 10 mM HEPES buffer.

1.3.2) Retrieve the slide from N<sub>2</sub> storage and clean it using RIE with the parameter setting: 500-Torr pressure, 100-W power, and 90-s duration.

1.3.3) Pipette one drop of passivating solution onto a piece of paraffin film.

1.3.4) Sandwich the solution with the film and the slide, making sure that the side with the pattern features is facing down towards the film; avoid the formation of bubbles.

1.3.5) Wait for 45 min before removing the slide from the film.

1.3.6) Soak the slide consecutively in photoresist remover, photoresist remover and DI water (1:1), and DI water, and agitate it in an ultrasound bath for 90 s for each soak.

1.3.7) Dry the slide on a hotplate to remove the moisture before sealing it in a desiccator and storing it in a refrigerator.

### **1.4) Chip assembly**

1.4.1) Repeat steps 1.1.1-1.1.4, but with SU8-2025-negative photoresist and the parameter setting referred called the Microchem protocol<sup>18</sup>, to prepare a silicon mold with a photomask.

1.4.2) Fabricate a PDMS microchannel (40 mm x 25 mm x 5 mm, L x W x H) and a small PDMS slab (800 µm-wide groove structure) using soft lithography.

1.4.3) Punch the microchannel for fluid access ports and clean it with tape and then with IPA.

1.4.4) Shield the patterned area of the glass substrate with the PDMS slab, and apply RIE (100 W, 500 mTorr, 60 s) to remove PLL-g-PEG from the peripheral area.

1.4.5) Treat the microchannel with a reduced dose of RIE (25 W, 500 mTorr, 25 s), and then align it to the patterned glass substrate (with the small PDMS slab removed); bring the microchannel and the patterned glass substrate in conformal contact under a stereoscope.



[Place Figure 3 here]

### **1.5) Cell attachment**

Note: HeLa cells are routinely maintained in DMEM supplemented with 10% FBS and 1% antibiotic/antimitotic solution in a cell culture incubator. A schematic diagram for the chip assembly and cell attachment is shown in Figure 3c.

1.5.1) Prime the chip with PBS for 30 min at 1  $\mu\text{L}/\text{min}$ , and then infuse fibronectin solution (50  $\mu\text{g}/\text{mL}$  in PBS, 1  $\mu\text{L}/\text{min}$ ) for 45 min.

1.5.2) While waiting, trypsinize cell culture with 0.25% trypsin-EDTA, wash them in culture medium, centrifuge individual cells, and reconstitute the cell suspension in pre-warmed (37  $^{\circ}\text{C}$ ) culture medium at  $5 \times 10^6$  cells/mL.

1.5.3) Replace the fibronectin solution with PBS and flush the chip at 10  $\mu\text{L}/\text{min}$  for 5 min.

1.5.4) Inject the prepared cell suspension into the chip, stop the flow, clamp the outlet, and maintain the chip in a cell culture incubator for 30 min.

1.5.5) Release the outlet and flush the chip with cell culture medium at 10  $\mu\text{L}/\text{min}$  for 5 min. Reduce the perfusion flow rate of the culture medium to 0.75  $\mu\text{L}/\text{min}$  and maintain the cell culture for 2 h in the incubator.

### **2. Bubble generation and flow visualization**

Note: A schematic of the experimental setup is shown in Figure 4a for tandem bubble generation and the resultant flow interaction with a single cell grown nearby in a microfluidic channel.

#### **2.1) Generation of tandem bubbles with two lasers and timing control**

2.1.1) Place the microfluidic chip on the stage of an inverted microscope and align the foci of two pulsed Nd:YAG lasers ( $\lambda = 532$  nm, 5-ns pulse duration) on a pair of patterned gold dots separated by 40  $\mu\text{m}$ .

2.1.2) Use a digital delay generator to trigger the two lasers with a time delay about 2.5  $\mu\text{s}$  to produce two bubbles initiated at the gold dots.

2.1.3) Adjust the laser output energy ( $\sim 10$   $\mu\text{J}$ ) to produce a maximum diameter of the bubbles within  $50 \pm 2$   $\mu\text{m}$ .

2.1.4) Synchronize a high-speed camera (200-ns exposure and 2 million frames per second (fps)) to the lasers and capture the dynamics of bubble expansion, collapse, bubble-bubble interaction, and jet formation.

## **2.2) Quantification of jet velocity**

2.2.1) Record the position of the jet tip ( $J_1$ ) at the proximal end of the first bubble ( $B_1$ ) and the distal end of  $B_1$ , starting at the generation of the second bubble ( $B_2$ ) and ending with the touchdown of  $J_1$  towards the distal end of  $B_1$ ; see the schematic in Figure 5a.

2.2.2) Linearly fit the time course of position for both the proximal (jet tip) and the distal ends. Calculate the slope of the tip position versus time curve for the proximal end to determine the jet speed. The intersection of the two lines indicates the jet touchdown time. More details can be found in Reference 19.

## **2.3) Visualization of the tandem bubble-induced flow field**

2.3.1) Prepare 1  $\mu\text{m}$  of polystyrene (PS) bead suspension in DI water (2.6% w/v) and inject the beads into the microfluidic chip.

2.3.2) Generate tandem bubbles (TBs) as described in step 2.1.1-2.1.3.

2.3.3) Record the TB dynamics using a high-speed video camera at a framing rate of 5 M fps with a 100-ns exposure time.

2.3.4) Upload the acquired image sequence into a commercial PIV software.

2.3.5) Divide each image into smaller interrogation windows of 16 x 16 pixels (px) with a 75% overlap.

2.3.6) Apply multi-pass iteration and regional filters to reduce the errors in velocity field computation, and output the results in a velocity vector map.

[Place Figure 4 here]

## **3. Single-cell analysis and bioeffects**

Note: The tandem bubble is produced next to the target cells, and the resultant bioeffects are studied in a standoff distance-dependent manner. The time sequence for different types of image acquisitions is depicted in Figure 4b.

### **3.1) Membrane poration and macromolecular uptake**

Note: The uptake of extracellular macromolecules into the target cell is characterized by the progressive diffusion of membrane impermeant propidium iodide (PI) through the poration site on the cell membrane.

3.1.1) Following step 1.5, replace the regular culture medium (*i.e.*, DMEM) with PI solution (100  $\mu\text{g/mL}$  in DMEM) running at a perfusion flow rate of 0.5  $\mu\text{L/min}$  throughout the experiment.

3.1.2) Program the microscope control software to automatically select the PI fluorescent cube on the rotating turret and synchronize the timing of the CCD camera with the PI fluorescence

excitation to capture fluorescence images with an exposure time of 200 ms.

3.1.3) After the two laser foci are aligned to a pair of gold dots next to a target cell, record both bright field (BF) and fluorescence (FL) images before the tandem bubble treatment.

3.1.4) Use microscope control software to immediately start a time-lapse fluorescence image recording of the target cell shortly after step 2.1 to capture the history of PI uptake.

### **3.2) Membrane deformation**

3.2.1) Prepare 1- $\mu$ m beads (1% w/v, activated with water-soluble carbodiimide) and functionalize them with Peptide-2000 (100  $\mu$ g/mL in PBS).

3.2.2) Following step 1.5, incubate the attached cells with the functionalized beads at a density of  $1 \times 10^9$  beads/mL at 37 °C for 30 min.

3.2.3) Repeat step 2.1 to produce TB next to the target cell and record the cell deformation with an ultra-high-speed camera running at a framing rate of 5 million fps.

3.2.4) Identify a triad of 3 beads that remain on the imaging plane throughout the experiment and compile their positions as  $(x_1, y_1)$ ,  $(x_2, y_2)$ , and  $(x_3, y_3)$  in the experiment coordinates.

3.2.5) Calculate the area of the triad before and after the TB treatment using the formula:

$$A = \sqrt{s(s-l_1)(s-l_2)(s-l_3)} = \frac{1}{2} |(-x_2y_1 + x_3y_1 + x_1y_2 - x_3y_2 - x_1y_3 + x_2y_3)|$$

3.2.6) Calculate the area strain as:

$$e_A = (A / A_0 - 1) = (1 + e_1)(1 + e_2) - 1 = e_1 + e_2 + e_1e_2$$

3.2.7) Based on the coordinates of the three vertices before and after the TB treatment, calculate the local principal strain and area strain following established protocols<sup>20,21</sup>.

### **3.3) Viability and apoptosis**

Note: FITC Annexin V labels cells, including apoptotic ones, through the externalization of phosphatidylserine (green fluorescence). PI labels the nuclei of necrotic cells (red fluorescence). Bright field imaging is used to document cell morphology and to assist with the identification of cell viability and apoptosis.

3.3.1) Record the position of each treated cell in the microfluidic channel (facilitated by the address labels in the channel, see Figure 2b) while repeating step 3.1.

3.3.2) Incubate the treated cells in the cell culture medium for another 2 h before perfusing the chip with FITC Annexin V solution for 15 min. Positive cells display green fluorescence.

3.3.3) Repeat step 3.3.2 24 h after the TB treatment to study the long-term bioeffects in the targeted cells.

### **3.4) Calcium response**

3.4.1) Mix 3  $\mu\text{L}$  of fura-2 AM stock solution (1 mg/mL in DMSO) with 3  $\mu\text{L}$  of 10% w/v Pluronic F-127 in 500  $\mu\text{L}$  of reduced serum medium to prepare the final labelling solution (6  $\mu\text{M}$ ).

3.4.2) Following step 1.5, replace the cell culture medium with the labelling solution and incubate under room temperature in the dark for 40 min (1  $\mu\text{L}/\text{min}$  perfusion rate).

3.4.3) Refill the channel with the reduced serum medium (0.75  $\mu\text{L}/\text{min}$  perfusion rate) before starting the cell experiment.

3.4.4) Start ratiometric imaging (wavelength: 340/380 nm, 50-ms exposure) of the target cell using the commercial PTI system.

3.4.5) After 10 s of ratiometric imaging of the cell at resting level, produce TB as in step 2.1; first record with an interframe time (IFT) of 0.1 s for 1 min, then increase the IFT to 1 s for another min, and further increase to 5 s after 2 min.

3.4.6) Use the PTI software to calculate the ratio  $R = F_{340}/F_{380}$  in the region of interest (ROI), which is proportional to the intracellular calcium concentration.

### **REPRESENTATIVE RESULTS:**

The microfluidic platform described in this work can be used to investigate bubble-bubble interactions and to analyze a variety of cavitation-induced bioeffects at the single-cell level. Here, we present several examples to demonstrate a variety of experimental studies and bioassays that can be performed in our experimental system. We will first illustrate the transient interactions of tandem bubbles with the jet formation, the visualization of the resultant flow field, and the calculation of the jet speed (Figure 5a). We will then present examples of tandem bubble-induced localized cell membrane deformation (Figure 5b), pinpointed membrane poration with PI uptake (Figure 5c), and intracellular calcium response (Figure 5d). Other examples, such as cell viability and apoptosis assays, can be found in Reference 22.

Figure 5a shows an example of the TB interaction with the jet formation, captured by high-speed imaging, and the resultant flow field revealed by PIV. Specifically, following its maximal expansion, the collapse of the first bubble  $B_1$  (produced at 0  $\mu\text{s}$ ) is distorted asymmetrically by the rapid expansion of the second bubble  $B_2$  (produced at 2.5  $\mu\text{s}$ ), leading to the formation of an “upward” jet ( $J_1$ ) at 3.4  $\mu\text{s}$  and the subsequent jetting flow, shown at 5.4  $\mu\text{s}$ . The average jet speed is determined by the slope of a fitted line for the position of the proximal end (or pole) of  $B_1$  before touchdown (*i.e.*, contact with the distal end of  $B_1$ ) versus time. The average jet speed is found to increase from 20 to 58 m/s when the maximum diameter of  $B_2$  increases from 40 to 60  $\mu\text{m}$ . Based on the results of PIV analysis, the directional jetting flow around the tandem

bubble is on the order of 10 m/s and is confined within a width on the order of 10  $\mu\text{m}$ . It is thus capable of producing an impulsive and localized shear stress and stress gradient onto a target cell grown nearby.

Another example shown in Figure 5b illustrates the cell membrane deformation induced by the directional and localized jetting flow produced by the TB at standoff distance  $S_d = 40 \mu\text{m}$ . The membrane deformation and recovery are highlighted by the displacement of a functionalized bead (indicated by the yellow dotted line) attached to the leading edge of the cell membrane. The local area strain can be calculated from the coordinates of a triad of adjacent beads. A schematic of the calculated maximum area change at different locations on the cell surface is shown in the middle. The leading edge is primarily stretched (see the green circles), while the trailing edge or lateral sides of the cell are compressed (as indicated by the red circles), indicating heterogeneity in cell deformation produced by the TB-induced jetting flow. The temporal variation of the area strain at the cell leading edge is illustrated on the right. It is comprised of a few rapid oscillations in the beginning, followed by a large and sustained stretch for about 100  $\mu\text{s}$  (FWHM) and a subsequent gradual recovery on a time scale of several ms.

Furthermore, the large area strain and strain integral at the cell leading edge may be responsible for the cell membrane poration observed at small  $S_d$ , as shown in Figure 5c. At small  $S_d$  (*i.e.*, 10  $\mu\text{m}$ , or in some cases, 20  $\mu\text{m}$ ) and intermediate  $S_d$  (*i.e.*, the majority of 20 and 30  $\mu\text{m}$ ), a localized membrane disruption is induced, leading to a pinpoint uptake of extracellular PI into the cytosol. If the PI intensity inside the cell keeps increasing without saturation, necrosis occurs. In comparison, if the PI intensity is an order of magnitude lower and reaches a plateau within 10 s following the TB treatment, repairable poration with likely cell survival will occur, which is further supported by the minimal change in cell morphology. At large  $S_d$  (*i.e.*, 40  $\mu\text{m}$ ), negligible PI uptake is found following TB treatment, indicating negligible or non-poration. The cell can survive with regular growth and proliferation<sup>22</sup>. Overall, the results show a clear transition in cell response from necrosis, through repairable membrane poration, to non-poration in the range of  $S_d \approx 20\text{-}40 \mu\text{m}$ .

Finally, we show the results of ratiometric imaging of the intracellular calcium response elicited by tandem bubbles in individual cells at different  $S_d$ , especially in the sublethal range of  $S_d = 30\text{-}50 \mu\text{m}$  (Figure 5d). The intensity ratio is proportional to the amount of intracellular calcium. At small  $S_d$  (*i.e.*, 30  $\mu\text{m}$  or, in some cases, 40  $\mu\text{m}$ ), a calcium wave travelling from the leading edge to the trailing edge is clearly observed within a few seconds following the tandem bubble treatment. After the intracellular calcium reaches a peak concentration, it decays slowly back to the resting level within a few minutes. In contrast, at large  $S_d$  (*i.e.*, a majority of 50  $\mu\text{m}$ , or in some cases, 40  $\mu\text{m}$ ), the increase of intracellular calcium is much milder, and no clearly-visible travelling calcium wave can be identified. These two different calcium responses can also be distinguished from their intensity ratio versus time profiles, with significant differences in the peak amplitude of the intensity ratio and the rise time from resting level to peak value. At an even larger  $S_d$  (*i.e.*, above 60  $\mu\text{m}$ ), no calcium response can be observed. The percentage of HeLa cells displaying calcium responses at various  $S_d$  is summarized in Figure 5C.

All in all, our results have demonstrated that, by altering the strength of the jetting flow (or changing  $S_d$ ), a variety of bioeffects can be produced in individual HeLa cells under similar culture conditions, which is likely correlated with the amplitude and duration of the mechanical deformation imposed on the cell membrane<sup>22</sup>.

**Figure 1: The microfluidic chip and schematics of different assays.**

**a)** An assembled microfluidic chip with channels filled with blue ink for visualization. **b)** A region inside the microfluidic chip with patterned cells and gold dots (the distance between the two gold dots in proximity is 40  $\mu\text{m}$ ). Many pairs of working units can be arranged in a channel. **c)** Close-up image of a single working unit consisting of a pair of gold dots and a HeLa cell adhered to the cell-patterning region. **d)** Schematic of the device operation. A single cell adheres to and spreads on the “H”-shaped island coated with fibronectin. A pair of cavitation bubbles (tandem bubble) with anti-phase oscillation are produced by illuminating pulsed laser beams on the gold dots (see Figure 4a), leading to the generation of a fast and localized jet moving towards the target cell nearby. The cell may be deformed, porated for macromolecular uptake, and/or stimulated with a calcium response, depending upon the standoff distance ( $S_d$ ) of the cell to the tandem bubble.

**Figure 2: Schematic of the channel design in the microfluidic chip and the dimensions of the working units.**

**a)** Mask design of the aligned PDMS microchannels (green) and the patterns on the glass substrate (blue and red). **b)** Enlarged image of the mask design in a representative section of the working unit arrays. **c)** Schematic of one working unit showing a cell pattern (blue) and a pair of gold dots (red). All the length scales are shown on the bottom right.

**Figure 3: Schematic diagrams for microfabrication and chip assembly.**

**a)** Pattern of gold dots on the glass substrate. **b)** Preparation of the glass substrate for cell patterning via MAPL. **c)** Assembly of the microfluidic channel with plasma bonding. See the materials table for the definitions of the abbreviations.

**Figure 4: Schematic of the experimental setup and image recording.**

**a)** Experimental setup for tandem bubble generation. **b)** Time sequence used for different types of imaging acquisitions. FL: fluorescence microscopy, BF: bright field, IFT: interframe time.

**Figure 5: Results from tandem bubble interaction, cell membrane deformation, membrane poration, and calcium response assays.**

Representative results. **a)** Fluid motion and the jet induced by tandem bubble interaction. Left: Selected frames showing tandem bubble interactions with the jet formation and flow field revealed by PIV. The maximum diameters of the two bubbles are about  $50 \pm 2 \mu\text{m}$ . Middle: Schematic of the jetting tandem bubbles, illustrating the center axis, origin of the coordinates ( $o$ ), and proximal and distal ends (or poles) of the first bubble  $B_1$ . Right: Measured pole positions (with error =  $\pm 1 \mu\text{m}$ ) at the proximal and distal end of  $B_1$ . **b)** Cell membrane deformation. Left: The yellow dotted line labels the displacement of a PS bead attached to the leading edge of the cell membrane, indicating the local membrane deformation and recovery.

Middle: a schematic showing the peak area strains at different locations on the cell surface shown on the left. Right: The time courses of the area strains in the middle of the cell leading edge.  $\Delta\epsilon$  is the area strain calculated based on principal strains and  $\Delta\Delta$  is the area strain calculated based on the triad geometry change. More details about the area strain calculation and error analysis are documented in Reference 22. **c)** Cell membrane poration. Left: bright field images before and after tandem bubble treatment and time-lapse fluorescence images of PI uptake (0 and 120 s). The white arrows indicate the jetting flow direction. Middle: the typical change of average PI intensity versus time inside the cells. Right: Statistical results of the percentage of cells undergoing necrosis (red), repairable poration (blue), and non-poration (green) at different  $S_d$ . Number of cells treated:  $N = 9, 14, 14,$  and  $8$  for  $SD = 10, 20, 30,$  and  $40$ , respectively. The statistic error is  $\pm 1/\sqrt{N}$ . **d)** Intracellular calcium response. Left: sequences of ratiometric images showing the intracellular calcium responses of individual cells at  $S$  of  $30\ \mu\text{m}$  and  $50\ \mu\text{m}$ . The red arrows indicate the jet direction. Middle: typical response profiles (ratio-time curves) at different  $S_d$ . Right: the probability of a calcium response at different  $S_d$ .

**Table 1: A list of parameters for flow physics from the PIV results.**

Estimated Reynolds number and averaged shear stress with respect to different standoff distances ( $S_d$ ). The YZ plane refers to the channel width x height plane. The averaged shear stress is estimated from a height of  $0$  to  $7.7\ \mu\text{m}$  from the channel bottom because the cell height in the channel is around  $6\text{-}7\ \mu\text{m}$ .

**DISCUSSION:**

Single-cell analysis, in combination with live-cell imaging, has greatly enhanced our understanding of the dynamic and often variable processes in individual cells, such as phenotype development and immune response<sup>23</sup>. In contrast to the conventional cell culture in dishes or flasks, microfluidic systems enable precise control of the microenvironment, down to the single-cell level, in real time. Consequently, advances in microfluidic technology and techniques have largely improved the throughput and reproducibility of single-cell analysis. By integrating soft lithography and surface patterning, microfluidic systems can be further designed to facilitate the in-depth analysis of a single cell's response to complex patterns of spatiotemporally-variable stimuli. For example, transient chemical or mechanical cues have been successfully delivered to single cells while their biological or mechanical responses were automatically recorded and analyzed<sup>24</sup>. Despite this general trend, the application of microfluidics to analyzing cavitation-induced bioeffects at the cellular level has been very limited. Most notably, it has only been applied to bubble-induced membrane poration of individual cells in suspension trapped by micropillars<sup>11</sup>. In the majority of studies on adherent cells, the benefit of controlling cell morphology to maintain consistency in dynamic bubble-cell interactions is either unavailable or largely neglected.

We have developed a microfluidic system to precisely control the initiation, subsequent expansion, and collapse dynamics of cavitation bubbles; bubble-bubble interactions with jet formation; and cell shape, orientation, adhesion pattern, and standoff distance from the bubbles, thus allowing for reproducible jetting flow to be applied to individual cells under well-controlled experimental conditions. This novel microfluidic system is ideal for carrying out

fundamental studies on cavitation bubble(s)–cell interactions that are relevant to a diverse range of therapeutic ultrasound applications, such as SWL, HIFU, and sonoporation. We have demonstrated that our microfluidic system can be used to investigate various cavitation-induced bioeffects, including cell membrane deformation, membrane poration, viability and calcium response, in a more controllable and reproducible manner. Most notably, the directional jetting flow produced by tandem bubbles allows us to probe the mechanical property and calcium response in individual cells under high strain-rates that have not been well characterized. The localized, impulsive mechanical stress produced by such a jetting flow cannot be achieved by conventional stretching methods, such as micropipette aspiration<sup>25</sup> and the use of optical<sup>26</sup> and magnetic tweezers<sup>27</sup>. Furthermore, in contrast to previous studies using ultrasound contrast agents<sup>8,28-30</sup> or laser-induced single bubbles<sup>31,32</sup>, our microfluidic system offers better control of cell geometry and adhesion conditions, thus reducing their substantial effect on cellular response and bioeffects<sup>16</sup>.

While our technique is reliable and reproducible, one must follow the protocol cautiously to ensure that the experimental system is faithfully reproduced. The quality of surface patterning in the microchannel is primarily responsible for the reproducibility of the bubble-bubble-cell interactions and the cascade of downstream bioeffects. For example, for HeLa cells, the area of each gold dot must be around 25-30  $\mu\text{m}^2$  to ensure stable bubble generation while preventing the cells from adhering. On the other hand, the area of each fibronectin-coated island has to be around 700-900  $\mu\text{m}^2$  to facilitate the adequate spreading of a single cell in a square while reducing the chance of multiple cells forming aggregates on the island. Alignment between the gold dots and the fibronectin-coated islands must be precisely performed with the aid of the mask aligner to keep the angular error within 1° and the axial error within 0.5  $\mu\text{m}$ . Moreover, this experimental system provides versatility in monitoring a series of events, with their time scale varied by orders of magnitude (*e.g.*, bubble dynamics:  $\mu\text{s}$ , cell deformation:  $\text{ms}$ , membrane poration:  $\text{s}$ , apoptosis:  $\text{h}$ ). Therefore, it is important to accurately control the timing of the image acquisition and recording of each sequence by fine-tuning the trigger signals (controlled by a digital delay generator). The single-cell culture must be well maintained in the microchannel to minimize cell-to-cell variation in phenotype (mostly referred to as morphology). Therefore, a minimum 2-h incubation is required for cell attachment and spreading on the islands before proceeding with downstream cell treatment. It is recommended to always keep the flow rate in the microchannel under 3  $\mu\text{L}/\text{min}$ , so that the flow shear stress produced by the circulating culture medium on the cell is within the physiological range.

One current limitation of our technique is that tandem bubble interaction and the resultant jetting flow can only be applied to a target cell once, because the gold dots will be ablated by the laser irradiation. This drawback limits the ability of our experimental system to mimic the bioeffects produced by therapeutic ultrasound, where cells are often exposed to cavitation events. However, this temporal limitation may be alleviated by applying another thin layer of silicon dioxide to protect the gold dots from direct exposure in the liquid<sup>15</sup>. Overall, our microfluidic system offers well-controlled experimental conditions to investigate the bioeffects produced from cavitation bubble(s)-cell interactions and has several unique features. First, both



the size and the location of the cavitation bubbles in our experimental system can be precisely controlled by adjusting the incident laser energy absorbed by the gold dots. Second, the geometry and adhesion of individual cells are standardized by cell patterning to minimize their effects on cell responses and bioeffects, leading to more reproducible results. Third, the parallel working units in the microfluidic chip design make it feasible to study downstream bioeffects, such as cell growth, proliferation, and potentially gene expression, after cavitation exposure, since each cell can be addressed and monitored individually. In summary, our microfluidic system and methodology create reliable bubble-bubble interactions to study the bioeffects of individual cells with improved precision.

Our current chip is designed for the analysis of individual HeLa cells. However, a modification of the pattern islands for other mammalian cell lines are also possible. Several improvements can be made to further broaden the applications of the chip. For example, substitutes of the PLL-g-PEG molecules could be explored to stop individual patterned cells from migrating even after 24 h. In addition, new chip designs with microfluidic valves may be explored to control the local microenvironment of the cells, so that chemicals such as fluorescence markers or toxic reagents will only be applied to a specific location, without affecting the cells in other regions of the chip. With these improvements, the microfluidic system presented here may provide opportunities to study the long-term bioeffects of single cells, such as metabolism, segregation, differentiation, and gene expression, following cavitation exposure or mechanical stimuli produced by an impulsive flow.

#### **ACKNOWLEDGMENTS:**

We would like to acknowledge the use of the clean room facility SMIF at Duke University. We also want to thank Hao Qiang for his assistance in measuring the jet velocity. The authors thank Todd Rumbaugh of Hadland Imaging for providing the Shimadzu HPV-X camera used in this study. The work was funded in part by NIH through grants 5R03EB017886-02 and 4R37DK052985-20.

#### **DISCLOSURES:**

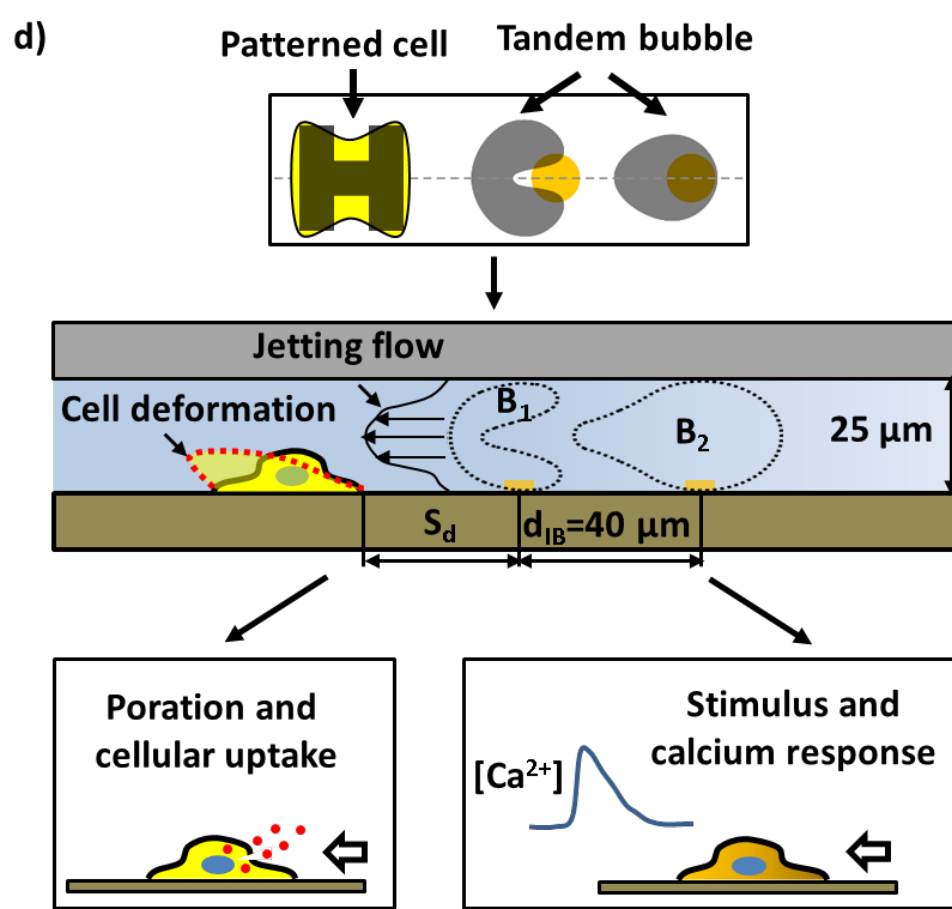
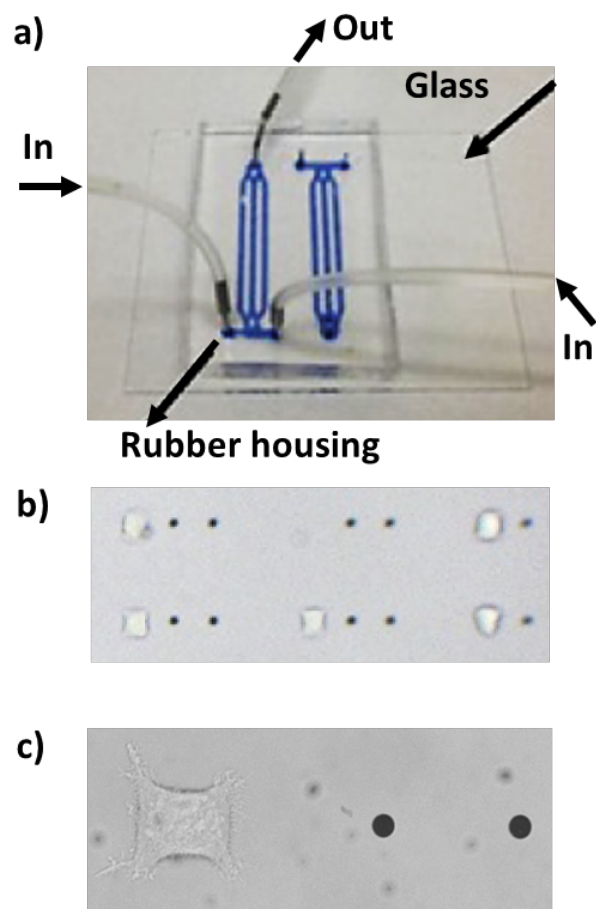
The authors have nothing to disclose.

#### **REFERENCES:**

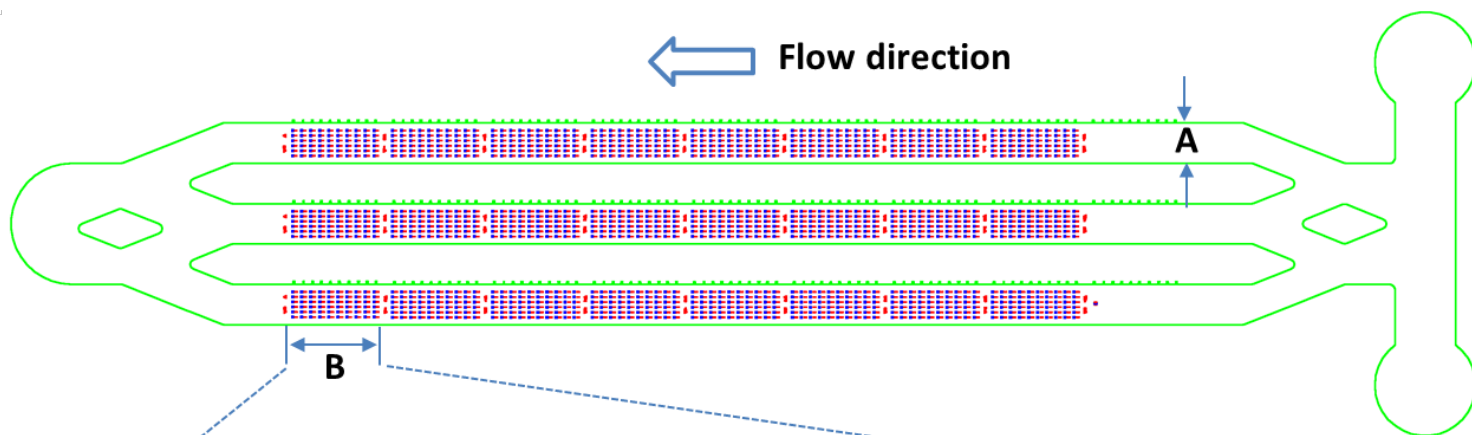
- 1 Wang, D. & Bodovitz, S. Single cell analysis: the new frontier in 'omics'. *Trends Biotechnol.* **28** (6), 281-290, doi:10.1016/j.tibtech.2010.03.002 (2010).
- 2 Weaver, W. M. *et al.* Advances in high-throughput single-cell microtechnologies. *Curr Opin Biotechnol.* **25** 114-123, doi:10.1016/j.copbio.2013.09.005 (2014).
- 3 Gossett, D. R. *et al.* Hydrodynamic stretching of single cells for large population mechanical phenotyping. *Proc Natl Acad Sci USA.* **109** (20), 7630-7635, doi:10.1073/pnas.1200107109 (2012).
- 4 Spiller, D. G., Wood, C. D., Rand, D. A. & White, M. R. H. Measurement of single-cell dynamics. *Nature.* **465** (7299), 736-745, doi:10.1038/nature09232 (2010).
- 5 Lecault, V., White, A. K., Singhal, A. & Hansen, C. L. Microfluidic single cell analysis: from promise to practice. *Curr Opin Chem Biol.* **16** (3-4), 381-390,

- doi:10.1016/j.cbpa.2012.03.022 (2012).
- 6 Kennedy, J. E. High-intensity focused ultrasound in the treatment of solid tumours. *Nat Rev Cancer*. **5** (4), 321-327, doi:10.1038/nrc1591 (2005).
- 7 Zhu, S., Cocks, F. H., Preminger, G. M. & Zhong, P. The role of stress waves and cavitation in stone comminution in shock wave lithotripsy. *Ultrasound Med Biol*. **28** (5), 661-671 (2002).
- 8 Fan, Z., Liu, H., Mayer, M. & Deng, C. X. Spatiotemporally controlled single cell sonoporation. *Proc Natl Acad Sci U S A*. **109** (41), 16486-16491, doi:10.1073/pnas.1208198109 (2012).
- 9 Itah, Z. *et al.* Hydrodynamic cavitation kills prostate cells and ablates benign prostatic hyperplasia tissue. *Exp Biol Med*. **238** (11), 1242-1250, doi:10.1177/1535370213503273 (2013).
- 10 Kosar, A., Sesen, M., Oral, O., Itah, Z. & Gozuacik, D. Bubbly cavitating flow generation and investigation of its erosional nature for biomedical applications. *IEEE Trans Biomed Eng*. **58** (5), 1337-1346, doi:10.1109/TBME.2011.2107322 (2011).
- 11 Li, Z. G., Liu, A. Q., Klaseboer, E., Zhang, J. B. & Ohl, C. D. Single cell membrane poration by bubble-induced microjets in a microfluidic chip. *Lab Chip*. **13** (6), 1144-1150, doi:10.1039/c3lc41252k (2013).
- 12 Li, F. F., Chan, C. U. & Ohl, C. D. Yield Strength of Human Erythrocyte Membranes to Impulsive Stretching. *Biophys J*. **105** (4), 872-879, doi:DOI 10.1016/j.bpj.2013.06.045 (2013).
- 13 Li F, M. M., Ohl CD. Shear stress induced stretching of red blood cells by oscillating bubbles within a narrow gap. *Bull Am Phys Soc*. **58**, doi:2013APS..DFDD11004L (2013).
- 14 Sankin, G. N., Yuan, F. & Zhong, P. Pulsating tandem microbubble for localized and directional single-cell membrane poration. *Phys. Rev. Lett*. **105** (7), 078101, doi:10.1103/PhysRevLett.105.078101 (2010).
- 15 Fan, Q., Hu, W. & Ohta, A. T. Laser-induced microbubble poration of localized single cells. *Lab Chip*. **14** (9), 1572-1578, doi:10.1039/C3LC51394G (2014).
- 16 Chen, C. S., Mrksich, M., Huang, S., Whitesides, G. M. & Ingber, D. E. Geometric control of cell life and death. *Science*. **276** (5317), 1425-1428, doi:10.1126/science.276.5317.1425 (1997).
- 17 Yuan, F., Sankin, G. & Zhong, P. Dynamics of tandem bubble interaction in a microfluidic channel. *J Acoust Soc Am*. **130** (5), 3339-3346, doi:10.1121/1.3626134 (2011).
- 18 Microchem. *SU-8 2000 Processing Guidelines*.
- 19 Yang, C. *Analysis of Tandem Bubble Interaction and Jet Formation in a Microfluidic Channel*, Duke University (2013).
- 20 Simon, S. I. & Schmid-Schonbein, G. W. Cytoplasmic strains and strain rates in motile polymorphonuclear leukocytes. *Biophys J*. **58** (2), 319-332, doi:10.1016/S0006-3495(90)82379-1 (1990).
- 21 Barbee, K. A., Macarak, E. J. & Thibault, L. E. Strain measurements in cultured vascular smooth muscle cells subjected to mechanical deformation. *Ann Biomed Eng*. **22** (1), 14-22 (1994).
- 22 Yuan, F., Yang, C. & Zhong, P. Cell membrane deformation and bioeffects produced by tandem bubble-induced jetting flow. *Proc. Natl. Acad. Sci. U.S.A.* **112** (51), E7039-E7047,

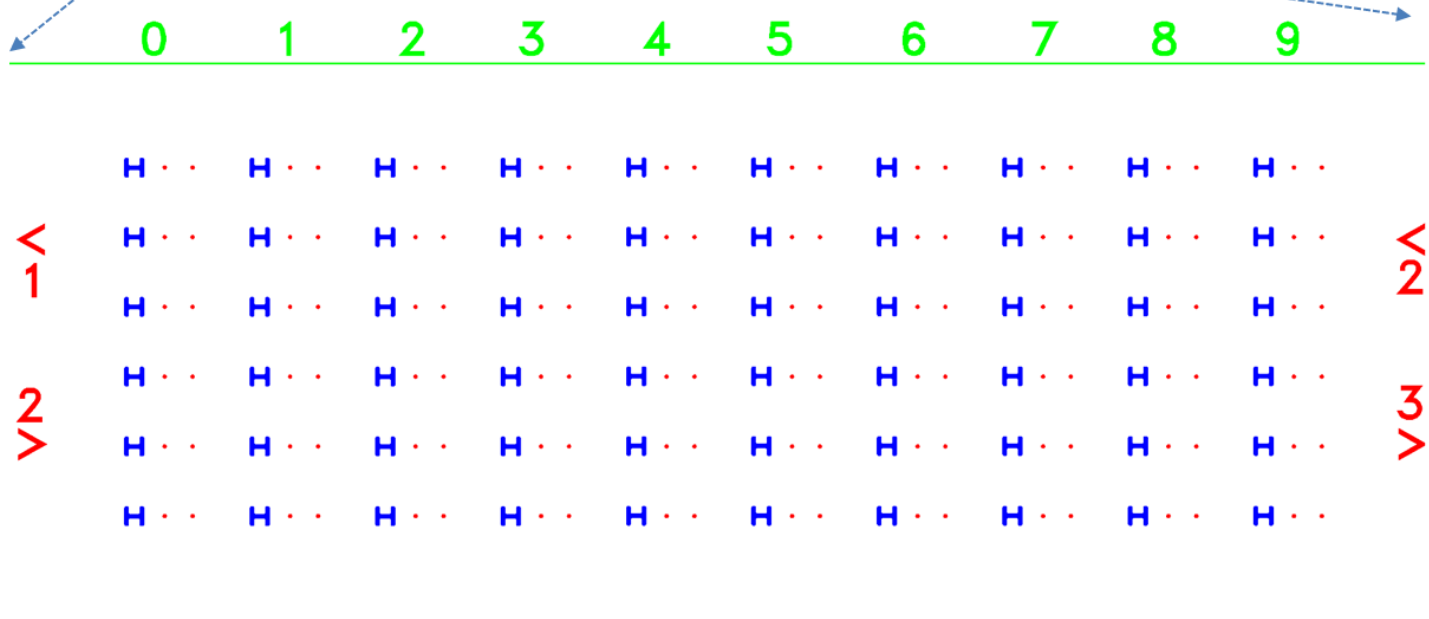
- doi:10.1073/pnas.1518679112 (2015).
- 23 Yin, H. & Marshall, D. Microfluidics for single cell analysis. *Curr Opin Biotechnol.* **23** (1), 110-119, doi:10.1016/j.copbio.2011.11.002 (2012).
- 24 Tay, S. *et al.* Single-cell NF-kappa B dynamics reveal digital activation and analogue information processing. *Nature.* **466** (7303), 267-U149, doi:10.1038/nature09145 (2010).
- 25 Rand, R. P. & Burton, A. C. Mechanical Properties of the Red Cell Membrane: I. Membrane Stiffness and Intracellular Pressure. *Biophys J.* **4** (2), 115-135, doi:10.1016/S0006-3495(64)86773-4 (1964).
- 26 Lim, C. T., Dao, M., Suresh, S., Sow, C. H. & Chew, K. T. Large deformation of living cells using laser traps. *Acta Mater.* **52** (7), 1837-1845, doi:10.1016/j.actamat.2003.12.028 (2004).
- 27 Puig-de-Morales-Marinkovic, M., Turner, K. T., Butler, J. P., Fredberg, J. J. & Suresh, S. Viscoelasticity of the human red blood cell. *Am J Physiol Cell Physiol.* **293** (2), C597-605, doi:10.1152/ajpcell.00562.2006 (2007).
- 28 Kudo, N., Okada, K. & Yamamoto, K. Sonoporation by single-shot pulsed ultrasound with microbubbles adjacent to cells. *Biophys J.* **96** (12), 4866-4876, doi:10.1016/j.bpj.2009.02.072 (2009).
- 29 van Wamel, A. *et al.* Vibrating microbubbles poking individual cells: Drug transfer into cells via sonoporation. *J Control Release.* **112** (2), 149-155, doi:10.1016/j.jconrel.2006.02.007 (2006).
- 30 Hu, Y., Wan, J. M. & Yu, A. C. Membrane perforation and recovery dynamics in microbubble-mediated sonoporation. *Ultrasound Med Biol.* **39** (12), 2393-2405, doi:10.1016/j.ultrasmedbio.2013.08.003 (2013).
- 31 Dijkink, R. *et al.* Controlled cavitation-cell interaction: trans-membrane transport and viability studies. *Phys Med Biol.* **53** (2), 375-390, doi:10.1088/0031-9155/53/2/006 (2008).
- 32 Rau, K. R., Quinto-Su, P. A., Hellman, A. N. & Venugopalan, V. Pulsed laser microbeam-induced cell lysis: Time-resolved imaging and analysis of hydrodynamic effects. *Biophys J.* **91** (1), 317-329, doi:10.1529/biophysj.105.079921 (2006).



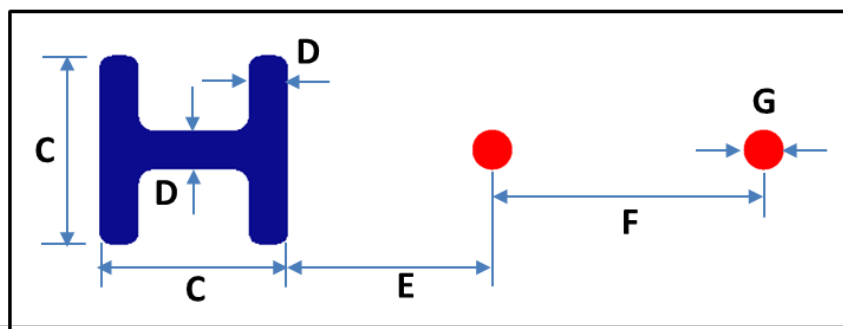
a)



b)

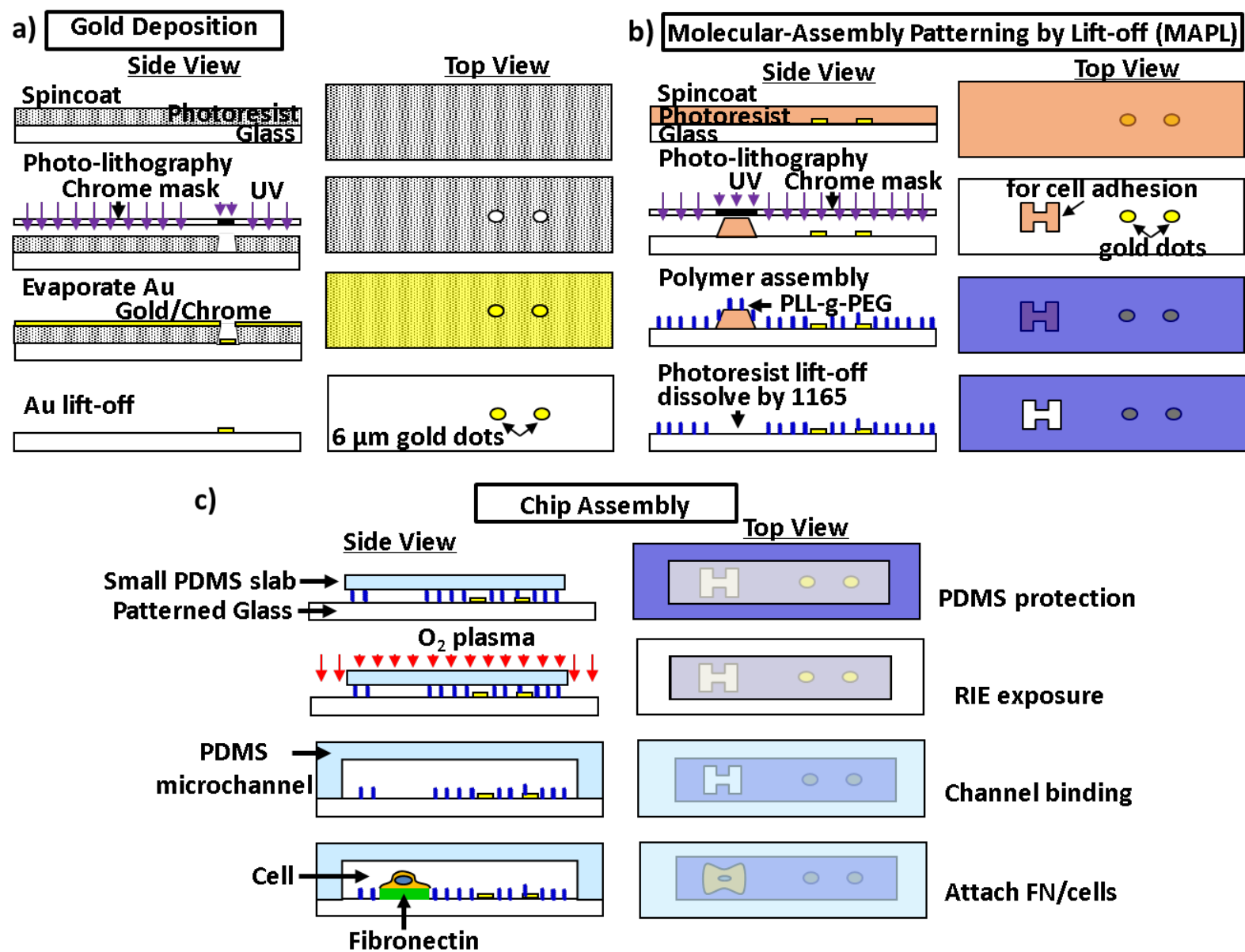


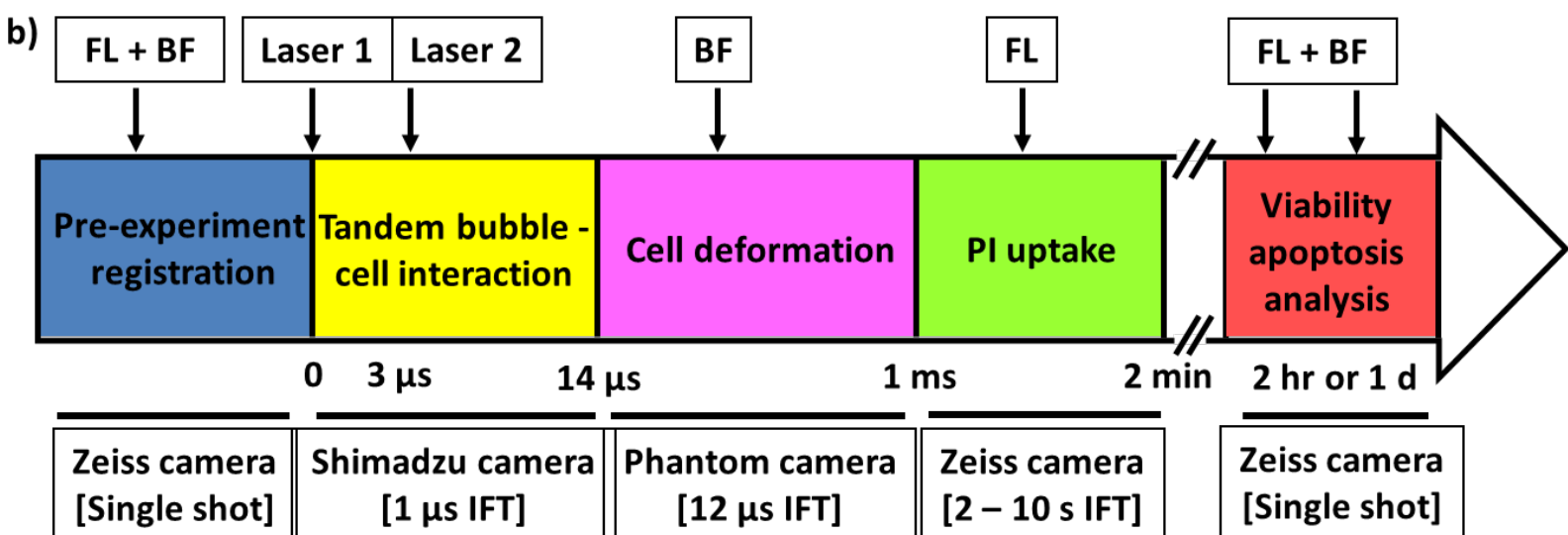
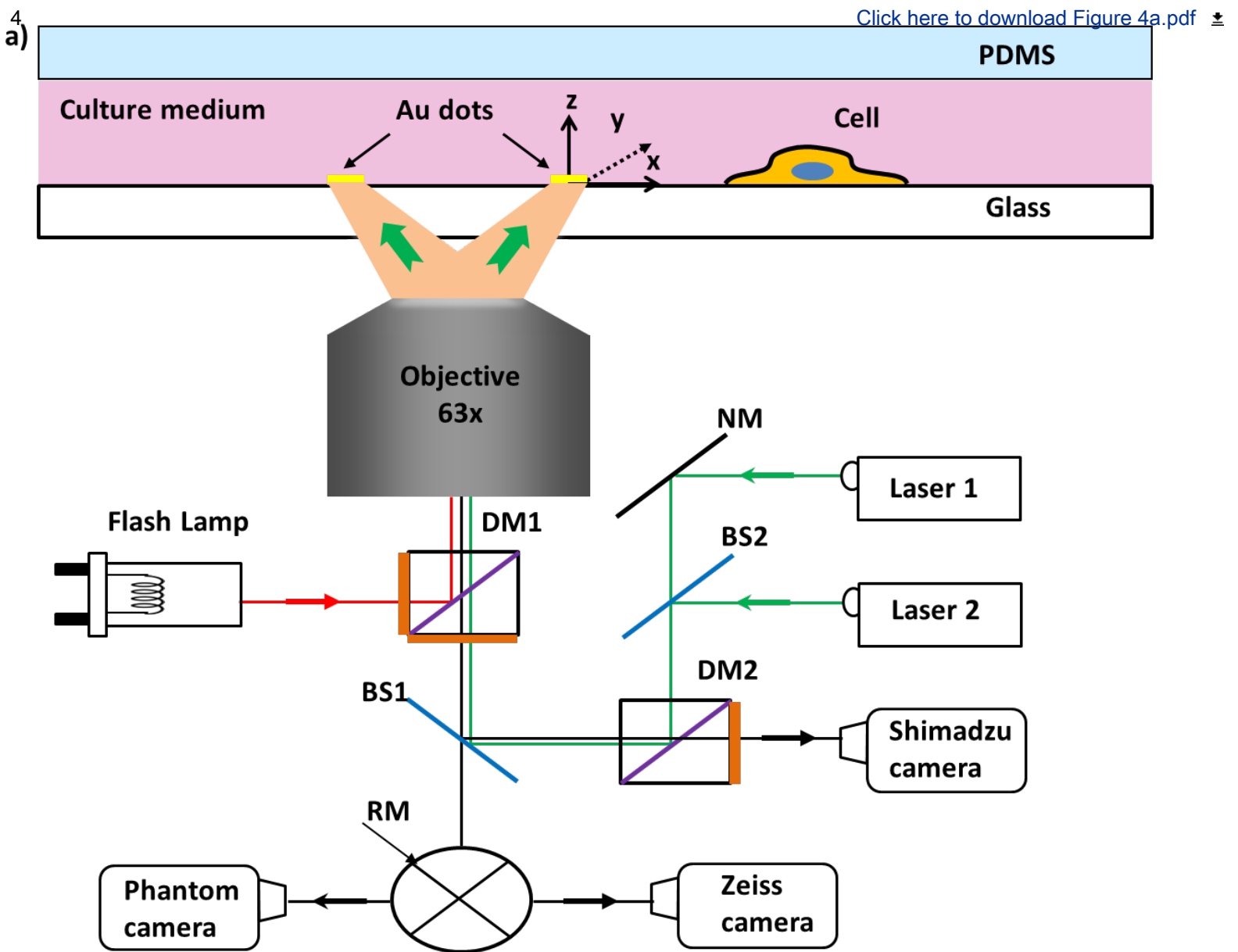
c)

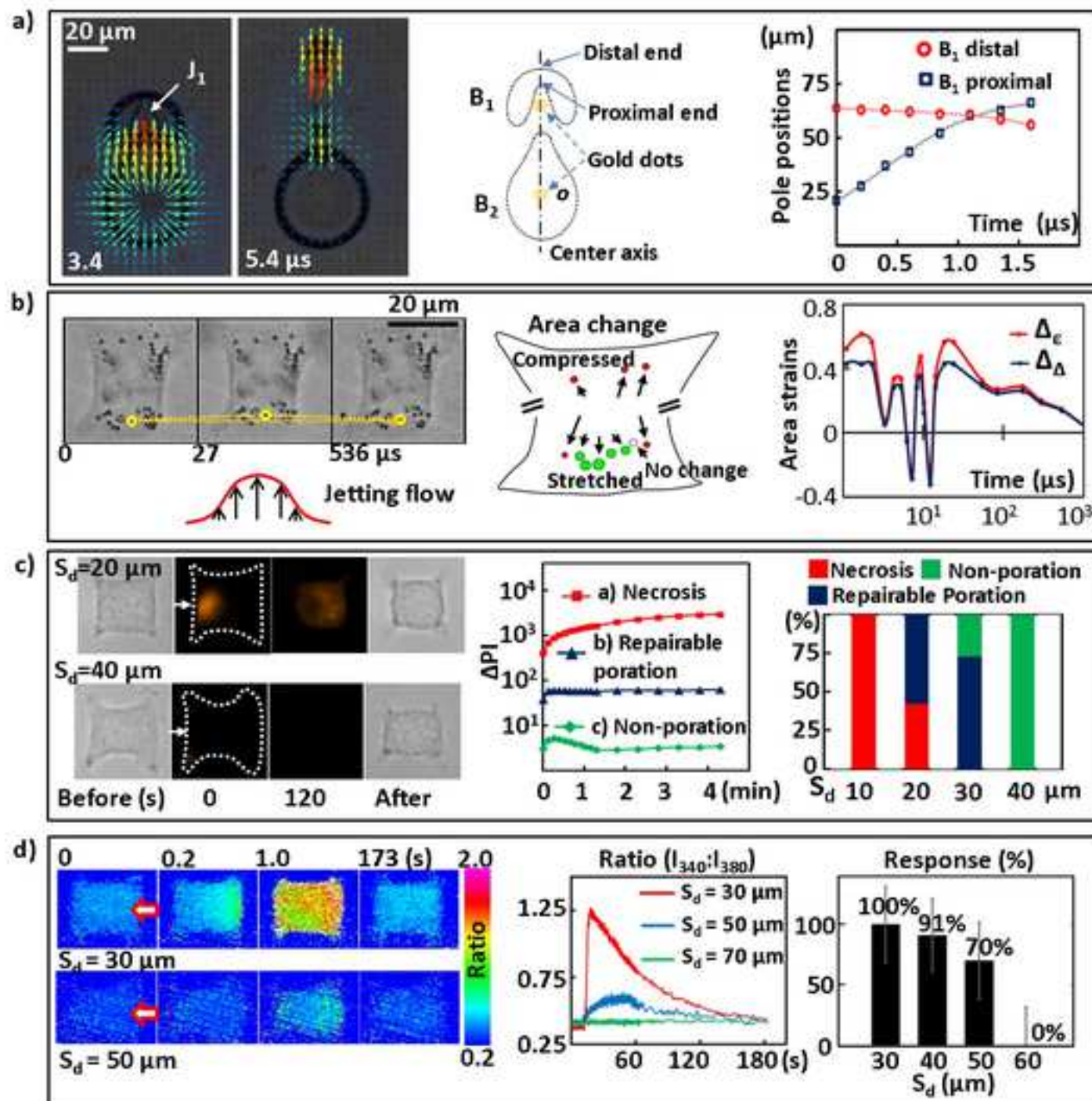
A: 800  $\mu\text{m}$ 

B: 2 mm

C: 32  $\mu\text{m}$ D: 8  $\mu\text{m}$ E: 10-70  $\mu\text{m}$ F: 40  $\mu\text{m}$ G: 6  $\mu\text{m}$









standoff distance (SD) ( $\mu\text{m}$ )	Reynolds number(Re)	averaged shear stress (Pa) in yz plane
20	206.96	618.64
30	354.8	709.69
40	378.78	657.22
50	163.85	323.61
60	105.08	42.21

Name of Reagent/Materials	Company	Catalog Number	Comments/Description
75x38mm Plain Microscope Slides	Corning	2947-75X38	
Acetone	Sigma Aldrich, Co.	320110	ACS reagent, ≥99.5%
Isopropyl alcohol	Sigma Aldrich, Co.	W292907	≥99.7%, FCC, FG
Sulfuric acid	Sigma Aldrich, Co.	320501	ACS reagent, 95.0-98.0%
Hydrogen peroxide	Sigma Aldrich, Co.	216763	30 wt.% in H2O
Primer P-20	Microchem	MCC Primer 80/20	
NFR photoresist	JSR	NFR016D2	
Photomask	Photoplotstore	N/A	4x4 Direct write mask
MF-319 Developer	Shipley (Rohm and Haas)	Microposit MF-319	
1165 Photoresist Remover	Dow Chemical, Co.	DEM-10018073	1-methyl-2-pyrrolidinone based
S1813 photoresist	Shipley (Rohm and Haas)	S1813	
PLL-g-PEG	SuSoS	PLL(20)-g[3.5]-PEG(2)	
HEPES	ThermoFisher Scientific	15630080	
Paraffin film	HACH	251764	
SU-2025 photoresist	Microchem	SU-2025	
PDMS	Dow Corning	184 SIL ELAST KIT 0.5KG	
Microbore Tubing	Saint-Gobain PPL Corp.	S-54-HL	
Metal pins	New England Small Tube	NE-1300-01	Cut Tube (straight), 0.025" OD x 0.017" ID x 0.50" Long
HeLa cells	Duke Cell Culture Facility	(307-CCL-2) HeLa, p.148	

DPBS(1X) buffer	ThermoFisher Scientific	14190144	
DMEM culture medium	ThermoFisher Scientific	11995065	
Fibronectin Bovine Protein, Plasma	ThermoFisher Scientific	33010018	
0.25% Trypsin-EDTA (1X)	ThermoFisher Scientific	25200056	
Propidium Iodide	ThermoFisher Scientific	P21493	
Carboxylate Microspheres 1.00µm	Polysciences, Inc	08226-15	
Carboxylate Microspheres 2.00µm	Polysciences, Inc	18327-10	
EDC (1-ethyl-3-(3-dimethylaminopropyl)carbodiimide hydrochloride)	ThermoFisher Scientific	22980	
Sulfo-NHS	Sulfo-NHS (N-hydroxysulfosuccinimide)	24510	
Peptide-2000	Advanced BioMatrix	5020-5MG	
FITC Annexin V	ThermoFisher Scientific	A13199	
Fura-2, AM	ThermoFisher Scientific	F1221	
DMSO	Sigma Aldrich, Co.	D2650	
F-127	invitrogen	P6866	0.2 µm filtered (10% Solution in Water)
Reduced serum media	ThermoFisher Scientific	11058021	

Name of Equipment	Company	model	Comments/Description
Plasma asher	Emitech	K-1050X	O2 / Ar plasma ashing of photoresist and other organic materials
Mask aligner	SUSS MicroTec	Karl Suss MA6/BA6	
E-beam evaporator	CHA Industries	CHA Industries Solution E-Beam	
RIE	Trion Technology	Trion Technology Phantom II	(oxide/ nitride/ polymer) etching
Stereoscope	AmScope	American Scope SM-4TZ-FRL	Stereo Microscope
Syringe pump	Chemyx Inc	NanoJet	
Cell culture incubator	NuAire	AutoFlow NU-8500 Water Jacket CO <sub>2</sub> Incubator	
Biological Safety Cabinets	NuAire	NU-425-400	
Water bath	VWR	1122s	
Centrifuge	IEC	Centra CL2	
Microscope	Zeiss	Axio Observer Z1	
Nd:YAG laser (laser 1)	New Wave Research	Tempest	
Nd:YAG laser (laser 2)	New Wave Research	Orion	
Delay generator	Berkeley Nucleonics	BNC 565-8c	
Flash lamp	Dyna-Lite	ML1000 fiber-coupled flashtube	
high speed camera	DRS Hadland	Imacon 200	
high speed camera	Shimadzu	HPV-X	
high speed camera	Vision Research	Phantom V7.3	
PIV software	LaVision	DaVis 7.2	

camera	Zeiss	AxioCam MRc 5	
software	Zeiss	AxioVision	
PTI system	Horiba	S/N: 1705 RAM-X	
EasyRatio software	Horiba	Easy Ratio Pro 2	version 2.3.125.86
63× objective	Zeiss	LD Plan Neofluar	



1 Alewife Center #200  
Cambridge, MA 02140  
tel. 617.945.9051  
www.jove.com

## ARTICLE AND VIDEO LICENSE AGREEMENT

Title of Article:

A Microfluidic System with Surface Patterning for Investigating Cavitation Bubble(s)-Cell Interaction and Resultant Bioeffects at Single Cell Level.

Author(s):

Fenfang Li, Fang Yuan, Georgii Sankin, Chen Yangji, Pei Zhong

Item 1 (check one box): The Author elects to have the Materials be made available (as described at <http://www.jove.com/publish>) via: ☒ Standard Access ☐ Open Access

Item 2 (check one box):

- ☒ The Author is NOT a United States government employee.
- ☐ The Author is a United States government employee and the Materials were prepared in the course of his or her duties as a United States government employee.
- ☐ The Author is a United States government employee but the Materials were NOT prepared in the course of his or her duties as a United States government employee.

### ARTICLE AND VIDEO LICENSE AGREEMENT

1. Defined Terms. As used in this Article and Video License Agreement, the following terms shall have the following meanings: “**Agreement**” means this Article and Video License Agreement; “**Article**” means the article specified on the last page of this Agreement, including any associated materials such as texts, figures, tables, artwork, abstracts, or summaries contained therein; “**Author**” means the author who is a signatory to this Agreement; “**Collective Work**” means a work, such as a periodical issue, anthology or encyclopedia, in which the Materials in their entirety in unmodified form, along with a number of other contributions, constituting separate and independent works in themselves, are assembled into a collective whole; “**CRC License**” means the Creative Commons Attribution-Non Commercial-No Derivs 3.0 Unported Agreement, the terms and conditions of which can be found at: <http://creativecommons.org/licenses/by-nc-nd/3.0/legalcode>; “**Derivative Work**” means a work based upon the Materials or upon the Materials and other pre-existing works, such as a translation, musical arrangement, dramatization, fictionalization, motion picture version, sound recording, art reproduction, abridgment, condensation, or any other form in which the Materials may be recast, transformed, or adapted; “**Institution**” means the institution, listed on the last page of this Agreement, by which the Author was employed at the time of the creation of the Materials; “**JoVE**” means MyJove Corporation, a Massachusetts corporation and the publisher of *The Journal of Visualized Experiments*; “**Materials**” means the Article and / or the Video; “**Parties**” means the Author and JoVE; “**Video**” means any video(s) made by the Author, alone or in conjunction with any other parties, or by JoVE or its affiliates or agents, individually or in collaboration with the Author or any other parties, incorporating all or any portion of the Article, and in which the Author may or may not appear.

2. Background. The Author, who is the author of the Article, in order to ensure the dissemination and protection of the Article, desires to have the JoVE publish the Article and create and transmit videos based on the Article. In furtherance of such goals, the Parties desire to memorialize in this Agreement the respective rights of each Party in and to the Article and the Video.

3. Grant of Rights in Article. In consideration of JoVE agreeing to publish the Article, the Author hereby grants to JoVE, subject to **Sections 4 and 7** below, the exclusive, royalty-free, perpetual (for the full term of copyright in the Article, including any extensions thereto) license (a) to publish, reproduce, distribute, display and store the Article in all forms, formats and media whether now known or hereafter developed (including without limitation in print, digital and electronic form) throughout the world, (b) to translate the Article into other languages, create adaptations, summaries or extracts of the Article or other Derivative Works (including, without limitation, the Video) or Collective Works based on all or any portion of the Article and exercise all of the rights set forth in (a) above in such translations, adaptations, summaries, extracts, Derivative Works or Collective Works and (c) to license others to do any or all of the above. The foregoing rights may be exercised in all media and formats, whether now known or hereafter devised, and include the right to make such modifications as are technically necessary to exercise the rights in other media and formats. If the “Open Access” box has been checked in **Item 1** above, JoVE and the Author hereby grant to the public all such rights in the Article as provided in, but subject to all limitations and requirements set forth in, the CRC License.



1 Alowife Center #200  
Cambridge, MA 02140  
tel. 617.945.9051  
www.jove.com

## ARTICLE AND VIDEO LICENSE AGREEMENT

4. Retention of Rights in Article. Notwithstanding the exclusive license granted to JoVE in **Section 3** above, the Author shall, with respect to the Article, retain the non-exclusive right to use all or part of the Article for the non-commercial purpose of giving lectures, presentations or teaching classes, and to post a copy of the Article on the Institution's website or the Author's personal website, in each case provided that a link to the Article on the JoVE website is provided and notice of JoVE's copyright in the Article is included. All non-copyright intellectual property rights in and to the Article, such as patent rights, shall remain with the Author.

5. Grant of Rights in Video – Standard Access. This **Section 5** applies if the "Standard Access" box has been checked in **Item 1** above or if no box has been checked in **Item 1** above. In consideration of JoVE agreeing to produce, display or otherwise assist with the Video, the Author hereby acknowledges and agrees that, Subject to **Section 7** below, JoVE is and shall be the sole and exclusive owner of all rights of any nature, including, without limitation, all copyrights, in and to the Video. To the extent that, by law, the Author is deemed, now or at any time in the future, to have any rights of any nature in or to the Video, the Author hereby disclaims all such rights and transfers all such rights to JoVE.

6. Grant of Rights in Video – Open Access. This **Section 6** applies only if the "Open Access" box has been checked in **Item 1** above. In consideration of JoVE agreeing to produce, display or otherwise assist with the Video, the Author hereby grants to JoVE, subject to **Section 7** below, the exclusive, royalty-free, perpetual (for the full term of copyright in the Article, including any extensions thereto) license (a) to publish, reproduce, distribute, display and store the Video in all forms, formats and media whether now known or hereafter developed (including without limitation in print, digital and electronic form) throughout the world, (b) to translate the Video into other languages, create adaptations, summaries or extracts of the Video or other Derivative Works or Collective Works based on all or any portion of the Video and exercise all of the rights set forth in (a) above in such translations, adaptations, summaries, extracts, Derivative Works or Collective Works and (c) to license others to do any or all of the above. The foregoing rights may be exercised in all media and formats, whether now known or hereafter devised, and include the right to make such modifications as are technically necessary to exercise the rights in other media and formats. For any Video to which this Section 6 is applicable, JoVE and the Author hereby grant to the public all such rights in the Video as provided in, but subject to all limitations and requirements set forth in, the CRC License.

7. Government Employees. If the Author is a United States government employee and the Article was prepared in the course of his or her duties as a United States government employee, as indicated in **Item 2** above, and any of the licenses or grants granted by the Author hereunder exceed the scope of the 17 U.S.C. 403, then the rights granted hereunder shall be limited to the maximum rights permitted under such

statute. In such case, all provisions contained herein that are not in conflict with such statute shall remain in full force and effect, and all provisions contained herein that do so conflict shall be deemed to be amended so as to provide to JoVE the maximum rights permissible within such statute.

8. Likeness, Privacy, Personality. The Author hereby grants JoVE the right to use the Author's name, voice, likeness, picture, photograph, image, biography and performance in any way, commercial or otherwise, in connection with the Materials and the sale, promotion and distribution thereof. The Author hereby waives any and all rights he or she may have, relating to his or her appearance in the Video or otherwise relating to the Materials, under all applicable privacy, likeness, personality or similar laws.

9. Author Warranties. The Author represents and warrants that the Article is original, that it has not been published, that the copyright interest is owned by the Author (or, if more than one author is listed at the beginning of this Agreement, by such authors collectively) and has not been assigned, licensed, or otherwise transferred to any other party. The Author represents and warrants that the author(s) listed at the top of this Agreement are the only authors of the Materials. If more than one author is listed at the top of this Agreement and if any such author has not entered into a separate Article and Video License Agreement with JoVE relating to the Materials, the Author represents and warrants that the Author has been authorized by each of the other such authors to execute this Agreement on his or her behalf and to bind him or her with respect to the terms of this Agreement as if each of them had been a party hereto as an Author. The Author warrants that the use, reproduction, distribution, public or private performance or display, and/or modification of all or any portion of the Materials does not and will not violate, infringe and/or misappropriate the patent, trademark, intellectual property or other rights of any third party. The Author represents and warrants that it has and will continue to comply with all government, institutional and other regulations, including, without limitation all institutional, laboratory, hospital, ethical, human and animal treatment, privacy, and all other rules, regulations, laws, procedures or guidelines, applicable to the Materials, and that all research involving human and animal subjects has been approved by the Author's relevant institutional review board.

10. JoVE Discretion. If the Author requests the assistance of JoVE in producing the Video in the Author's facility, the Author shall ensure that the presence of JoVE employees, agents or independent contractors is in accordance with the relevant regulations of the Author's institution. If more than one author is listed at the beginning of this Agreement, JoVE may, in its sole discretion, elect not take any action with respect to the Article until such time as it has received complete, executed Article and Video License Agreements from each such author. JoVE reserves the right, in its absolute and sole discretion and without giving any reason therefore, to accept or decline any work submitted to JoVE. JoVE and its employees, agents and independent contractors shall have



1 Alewife Center #200  
Cambridge, MA 02140  
tel. 617.945.9051  
www.jove.com

# ARTICLE AND VIDEO LICENSE AGREEMENT

full, unfettered access to the facilities of the Author or of the Author's institution as necessary to make the Video, whether actually published or not. JoVE has sole discretion as to the method of making and publishing the Materials, including, without limitation, to all decisions regarding editing, lighting, filming, timing of publication, if any, length, quality, content and the like.

11. **Indemnification.** The Author agrees to indemnify JoVE and/or its successors and assigns from and against any and all claims, costs, and expenses, including attorney's fees, arising out of any breach of any warranty or other representations contained herein. The Author further agrees to indemnify and hold harmless JoVE from and against any and all claims, costs, and expenses, including attorney's fees, resulting from the breach by the Author of any representation or warranty contained herein or from allegations or instances of violation of intellectual property rights, damage to the Author's or the Author's institution's facilities, fraud, libel, defamation, research, equipment, experiments, property damage, personal injury, violations of institutional, laboratory, hospital, ethical, human and animal treatment, privacy or other rules, regulations, laws, procedures or guidelines, liabilities and other losses or damages related in any way to the submission of work to JoVE, making of videos by JoVE, or publication in JoVE or elsewhere by JoVE. The Author shall be responsible for, and shall hold JoVE harmless from, damages caused by lack of sterilization, lack of cleanliness or by contamination due to the making of a video by JoVE its employees, agents or independent contractors. All sterilization, cleanliness or decontamination procedures shall be solely the responsibility of the Author and shall be undertaken at the Author's

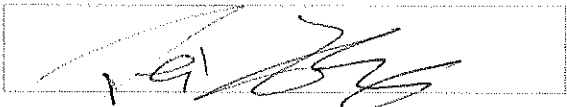
expense. All indemnifications provided herein shall include JoVE's attorney's fees and costs related to said losses or damages. Such indemnification and holding harmless shall include such losses or damages incurred by, or in connection with, acts or omissions of JoVE, its employees, agents or independent contractors.

12. **Fees.** To cover the cost incurred for publication, JoVE must receive payment before production and publication the Materials. Payment is due in 21 days of invoice. Should the Materials not be published due to an editorial or production decision, these funds will be returned to the Author. Withdrawal by the Author of any submitted Materials after final peer review approval will result in a US\$1,200 fee to cover pre-production expenses incurred by JoVE. If payment is not received by the completion of filming, production and publication of the Materials will be suspended until payment is received.

13. **Transfer, Governing Law.** This Agreement may be assigned by JoVE and shall inure to the benefits of any of JoVE's successors and assignees. This Agreement shall be governed and construed by the internal laws of the Commonwealth of Massachusetts without giving effect to any conflict of law provision thereunder. This Agreement may be executed in counterparts, each of which shall be deemed an original, but all of which together shall be deemed to be one and the same agreement. A signed copy of this Agreement delivered by facsimile, e-mail or other means of electronic transmission shall be deemed to have the same legal effect as delivery of an original signed copy of this Agreement.

A signed copy of this document must be sent with all new submissions. Only one Agreement required per submission.

## CORRESPONDING AUTHOR:

Name:	Pei Zhong	
Department:	Mechanical Engineering and Materials Science	
Institution:	Duke University	
Article Title:	A Microfluidic System with Surface Patterning for Investigating Cavitation Bubble(s)-Cell Interaction and Resultant Bioeffects at Single Cell Level.	
Signature:		Date: June 9th 2016

Please submit a signed and dated copy of this license by one of the following three methods:

- 1) Upload a scanned copy of the document as a pdf on the JoVE submission site;
- 2) Fax the document to +1.866.381.2236;
- 3) Mail the document to JoVE / Attn: JoVE Editorial / 1 Alewife Center #200 / Cambridge, MA 02139

For questions, please email [submissions@jove.com](mailto:submissions@jove.com) or call +1.617.945.9051



# Responses to Editorial and Peer Review Comments

## Editorial comments:

The manuscript has been modified by the Science Editor to comply with the JoVE formatting standard. Please maintain the current formatting throughout the manuscript. **The updated manuscript (55106\_R0\_061616.docx)** is located in your Editorial Manager account. In the revised PDF submission, there is a hyperlink for downloading the .docx file. **Please download the .docx file and use this updated version for any future revisions.**

Changes to be made by the Author(s):

1. Please take this opportunity to thoroughly proofread the manuscript to ensure that there are no spelling or grammar issues. The JoVE editor will not copy-edit your manuscript and any errors in the submitted revision may be present in the published version.

Reply:

We want to thank the editor for giving us this opportunity. We have proofread the manuscript, and corrected spelling and grammar errors.

2. Please abbreviate all journal titles.

Reply:

We have abbreviated all journal titles.

3. Please include volume, issue numbers, and DOIs for all references.

Reply:

These are included for all references now.

4. Please define all abbreviations before use.

Reply:

We have defined all abbreviations before use by adding brackets with abbreviations enclosed after the full expression.

5. Formatting:

-Please include spaces between numbers and units.

-All figure legends should have a title and a brief description. For Figure 3, all panels should

be described.

-References – Please abbreviate journal titles.

Reply:

We have taken care of these formatting issues. All panels are now described in the figure legend of Figure 3.

6. Grammar:

-Please copyedit the manuscript for numerous grammatical errors throughout. Such editing is required prior to acceptance. A few examples are listed below.

-Line 137: "yet small enough to avoid individual cells to adhere on it"

-1.1.3.2. "Set up the photolithography recipe in hard exposure mode with 9 s UV exposure. Moves directly to: "After UV exposure, bake the slide at 95 °C for 1min, and then let it cool down to room temperature." This is confusing, "set up" sounds like the action is preparing for, not carrying out the UV exposure. Please re-word here, and in 1.2.2.2

-1.1.5.2 – "Clean the slide in the reactive"

-1.1.5.6 – "Bake dry the slide before clean it"

-The discussion requires extensive editing for minor errors in grammar, particularly in article usage (a, an, the).

Reply:

We want to thank the editor for pointing out these errors. We have corrected these grammatical errors accordingly in the manuscript.

7. Visualization: Protocol is discontinuous. Please highlight a continuous protocol (that is, all steps in a section required for success of the protocol) are highlighted so that we can form a linear narrative. For instance, 1.2.2.2 and 1.2.2.5 should also be highlighted.

Reply:

Thank the editor for finding this issue. A more continuous protocol is now highlighted. For example, 1.2.2.2, 1.2.2.5, 1.2.3.1, and 1.3.1 are highlighted now.

8. Additional detail is required:

-1.1.2 – What speed/time is used for spin coating?

-1.1.5.2 – How is this performed? Please provide stepwise detail.

-1.1.5.3 – Please provide a citation or detail.

-2.2 – Please provide a citation.

Reply:

- 1.1.2 -The speed/time for spin-coating is described in 1.1.2.2;
- 1.1.5.2 –The slide is cleaned with plasma from the RIE machine, the parameter settings are already described.
- 1.1.5.3 –A related citation is now added for this step.
- 2.2-A citation is now provided.

9. Please remove all commercial branding:

-4.3.4 – Opti-MEM

-Please remove trademark symbols from the materials table.

Reply:

Opti-MEM has been removed from 3.4.1 and 3.4.3.

Trademark symbols are now removed from the materials table.

#### **Reviewers' comments:**

##### **Reviewer #1:**

###### *Manuscript Summary:*

This is a nice list of steps needed to conduct the experiments. Not sure how many people have 2 high-speed cameras and the bio and laser tools, yet it should help someone with the equipment and expertise to repeat the experiments. The experiments have been published extensively in a number of journals. Thus they are sound.

###### *Major Concerns:*

Very expensive experiment

###### **Response:**

We thank the reviewer for the supportive comments on the experimental protocols. The experimental system was set up initially to collect sufficient data to establish the correlation between bubble dynamics/jetting flow and cell deformation/bioeffects. The most expensive component of the system is the ultra high-speed camera; other expensive components such as the pulsed Nd: YAG lasers may be replaced by pulsed LEDs in the future since only about 10  $\mu$ J pulse energy is needed to generate a bubble in our system. Similarly, once the methodology is established, simple optical techniques (e.g., a linear array of photodiodes) can be used to measure maximum bubble size in real time, thus potentially eliminating the

need for an ultra high-speed camera. It is our ultimate goal to simplify the experimental system after the fundamental studies are completed.

*Minor Concerns:*

N/A

*Additional Comments to Authors:*

N/A

**Reviewer #2:**

*Manuscript Summary:*

In this study, cavitation bubble(s)-cell interaction and resultant bioeffects were investigated using a microfluidic system. The flow is characterized with PIV technique. The authors presented an interesting study and provided details on their experimental setup and procedure. They successfully combined fluid mechanics with biophysics, which constitutes the strength of the study. It also seems that the experiments were carefully performed and necessary discussion on the results is present. This study will make a fine contribution to the literature. However, there are some issues the authors should address.

**Response:**

Thank you very much for your supportive and encouraging comments.

*Major Concerns:*

1-Introduction: It is short for a journal article. It should be extended with recent biotechnology studies related to cavitation such as Hydrodynamic cavitation kills prostate cells and ablates benign prostatic hyperplasia tissue, Z Itah, et al., Experimental Biology and Medicine, 2013.

Bubbly cavitating flow generation and investigation of its erosional nature for biomedical applications

A Kosar et al., IEEE Transactions on Biomedical Engineering 58 (5), 1337-1346, 2011.

**Response:**

We have expanded the introduction with citation of these studies.

2-Were the cells tested under non-cavitating conditions? It would be nice to filter out shear effects due to liquid flow with control experiments.

**Response:**

We have tested the cells with liquid flow induced by single cavitation at 20  $\mu\text{m}$  standoff distance. The cell viability is 100%, with much weaker deformation and poration. Previously, we also tried liquid flow on cells without cavitation bubble. It turns out that liquid flow with no cavitation is even weaker than single bubble, which is similar to the reference<sup>1</sup> mentioned above.

3-It will be nice to include non-dimensional parameters such as Reynolds number, cavitation number, bubble to channel diameter ratio to represent the results. Thus, they could be converted to universal results.

Response:

The cavitation number is not applicable here because of the nature of laser-induced cavitation. Particularly, the water temperature is not constant in the laser focus that breaks the balance between the kinetic and potential energy in liquid.

Bubble to channel diameter ratio: bubble diameter/channel width =  $(50 \pm 2)/800 = 0.625 \pm 0.0025$ ;

We have added a table listing the standoff distance, Reynolds number and averaged shear stress into the manuscript.

4-What are the uncertainties in the experimental parameters? They should be included.

Response:

The statistic error is  $\pm 1/\sqrt{N}$ , N is the number of cells tested;

Bubble size  $50 \pm 2 \mu\text{m}$ ;

Standoff distance (SD):  $\pm 0.5 \mu\text{m}$ .

These information is now included into the manuscript.

5-The authors mentioned necrosis and apoptosis. How about autophagy? Does it play a role in this study?

Response:

Autophagy is related to the physiological process in the body that deals with destruction of cells. We are most interested in repairable membrane poration, which has potential for cavitation-targeted drug delivery, and mechanical stretch-induced calcium response that may be used for stimulating cell/tissue growth. Therefore, autophagy is beyond the scope of this study.

6-Cell-PIV particle bead interactions: Were such interactions present? If yes, how did the authors filter out these effects in their results?

Response:

The PIV beads are different from the RGD beads for cell membrane deformation. They are polystyrene beads without any surface functionalization, thus not able to attach to the cell membrane by integrin binding as the RGD beads. Besides, our PIV studies are performed without cells, thus PIV beads are not interacting with cells. We have added more description of the beads in the manuscript to distinguish these issues.

7-What are the stresses on the emerging bubbles and impact pressure upon bubble collapse? This info is necessary to make the results complete.

Response:

The estimated maximum shear stress in our setup is about 1 kPa, which is within the range of previously reported critical shear stress of 0.1 kPa for cell detachment<sup>2</sup> and water-hammer pressure of 3 kPa for jet impact induced membrane rupture<sup>3</sup>.

8-It will be nice to summarize the ranges for experimental parameters such as cavitation number, Reynolds number, diameter ratio, stresses in a separate table.

Response:

This comment is similar to comment #3. The cavitation number is not applicable to our study. We have listed other parameters (Reynolds number, diameter ratio, stresses) in a separate table.

9-More discussion about flow physics is necessary and should be linked to experimental results. The authors can borrow some from the studies on micro scale cavitating flows.

Response:

We have local stresses in our systems, and it is different with the global stresses from the studies on micro scale cavitating flows<sup>1,4</sup>.

The focus of this manuscript is the experimental protocols and representative results. More details about the flow physics and the correlation to experimental results can be found in our previous publications<sup>3,5</sup>.

*Minor Concerns:*

1-3.2.5-3.2.6: The equations should be formatted so that they would become clearer.

**Response:**

There is a display issue with the previous submission. We have taken care to make sure the equations are correctly formatted.

2-The quality of Fig. 5 should be improved.

3-More info about repeatability of experiments should be included.

4-It would be nice to include error bars in the figures.

**Response to comments 2-4:**

We have added error bars to Fig. 5d and specified the number of cells treated in Fig. 5c to improve the figure quality and clarify the repeatability of the experiments. For more details about the error analysis of the area strains calculation, please refer to our previous publication<sup>5</sup>.

*Additional Comments to Authors:*

N/A

**References**

- 1 Kosar, A., Sesen, M., Oral, O., Itah, Z. & Gozuacik, D. Bubbly cavitating flow generation and investigation of its erosional nature for biomedical applications. *IEEE Trans Biomed Eng.* **58** (5), 1337-1346, doi:10.1109/TBME.2011.2107322, (2011).
- 2 Ohl, C. D. & Ikink, R. Shock-wave-induced jetting of micron-size bubbles. *Phys Rev Lett.* **90** (21), 214502, doi:10.1103/PhysRevLett.90.214502, (2003).
- 3 Sankin, G. N., Yuan, F. & Zhong, P. Pulsating tandem microbubble for localized and directional single-cell membrane poration. *Physical Review Letters.* **105** (7), 078101, doi:10.1103/PhysRevLett.105.078101, (2010).
- 4 Itah, Z. *et al.* Hydrodynamic cavitation kills prostate cells and ablates benign prostatic hyperplasia tissue. *Exp Biol Med (Maywood).* **238** (11), 1242-1250, doi:10.1177/1535370213503273, (2013).

- 5 Yuan, F., Yang, C. & Zhong, P. Cell membrane deformation and bioeffects produced by tandem bubble-induced jetting flow. *Proceedings of the National Academy of Sciences*. **112** (51), E7039-E7047, doi:10.1073/pnas.1518679112, (2015).